A Vortex-Lattice Method for General, Unsteady Aerodynamics

P. Konstadinopoulos,* D. F. Thrasher,† D. T. Mook,‡ A. H. Nayfeh,‡ and L. Watson§
Virginia Polytechnic Institute and State University, Blacksburg, Virginia

A general method of calculating unsteady, incompressible, inviscid, three-dimensional flows around arbitrary planforms has been developed. The method is an extension of the vortex-lattice technique. It is not limited by aspect ratio, camber, or angle of attack, as long as vortex breakdown does not occur above the surface of the wing and separation occurs only along sharp edges. As the wing performs arbitrary maneuvers, the position of the wake and the distribution of circulation on the wing and in the wake are obtained as functions of time. One desirable feature of the present method is its ability to treat steady lifting flows very efficiently. Several examples of steady and unsteady flows are presented. These include rectangular wings, with and without flaps, delta, and cropped delta wings.

I. Introduction

THE well-known vortex-lattice method that has been used with considerable success to treat steady flows at low subsonic velocities can be extended to treat general unsteady flows. We will describe herein an extension that has evolved from work discussed in two earlier papers.[1,2]

The present method can be applied to three-dimensional lifting surfaces of any planform, camber, or twist. The surface may undergo any time-dependent deformation, and it can execute any maneuver in moving air. The only restrictions are that separation occurs along the sharp edges, vortex bursting does not occur near the surface, and the flow is incompressible. The method treats the position of, and the vortex distribution in, the wake as unknown. The method accounts for leading-edge separation on highly swept delta and delta-like wings, and for wing-tip vortex systems on low-aspect rectangular, swept, and tapered wings. In all calculations the recent history of the flow is taken into account. The results for the cases examined are in good agreement with available experimental data.

There is a considerable amount of still-growing literature devoted to unsteady aerodynamics. A great portion is devoted to the development of special, efficient techniques restricted to large aspect ratios, small angles of attack, and small-amplitude, simple-harmonic oscillations. For a discussion of many of these techniques, we refer to the review articles of Ashley and Rodden[3] and Belotserkovskii[4] and the recent papers by Ueda and Dowell[5] and Levin and Katz.[6] Though the method developed here can treat this important problem, the principal objective was the development of a method for general unsteady aerodynamics. The present method is a generalization of the familiar vortex-lattice method for steady, lifting flows. As such, it is relatively easy to use. Further discussion of the literature can be found in Ref. 7.

The current development differs from earlier methods in two significant ways: 1) The present method employs an explicit routine for generating the unsteady wakes (instead of the implicit scheme requiring iteration that was used earlier), thereby providing efficiency without a noticeable loss of accuracy, and 2) with the present method the problem is posed in terms of a body-fixed reference frame. The wing may be viewed as moving through air either at rest or in motion. Thus, the effects of gusts on a maneuver can be modeled. Moreover, the method can accommodate more than one body; thus, unsteady interference can be modeled with accurate estimates of the phasing among loads.

Received Feb. 7, 1984; revision received May 25, 1984.

*Graduate Research Assistant, Department of Engineering Science and Mechanics.

†Graduate Research Assistant; presently at the David Taylor Naval Ship Research and Development Center, Carderock, Md.

‡Professor. Member AIAA.

§University Distinguished Professor.

II. Description of the Method

A. General

Two coordinate frames—an inertial or ground-fixed (G-F) frame and a moving or body-fixed (B-F) frame—are used. The moving frame is attached to the wing and follows it through all of its maneuvers. If the wing is deforming, then this frame is attached to some reference configuration of the wing. The problem is posed in terms of the moving frame. The motion of the wing and the motion of the ambient fluid may be specified as arbitrary functions of time.

The two coordinate systems are shown in Fig. 1. The base vectors for the B-F frame (x,y,z) are denoted by $(\boldsymbol{i},\boldsymbol{j},\boldsymbol{k})$ and those for the G-F frame (X,Y,Z) by $(\boldsymbol{I},\boldsymbol{J},\boldsymbol{K})$. For the cases examined in this paper (flat plates), the x and z axes lie on the plane of the wing, while the y axis is perpendicular to the surface and points downward. The moving frame is originally aligned with the inertial frame. The important position vectors can be written in terms of their components as follows:

$$\boldsymbol{R}_A = X_A\boldsymbol{I} + Y_A\boldsymbol{J} + Z_A\boldsymbol{K}, \quad \boldsymbol{R} = X\boldsymbol{I} + Y\boldsymbol{J} + Z\boldsymbol{K},$$

$$\boldsymbol{r} = x\boldsymbol{i} + y\boldsymbol{j} + z\boldsymbol{k} \tag{1a}$$

It follows from Fig. 1 that

$$\boldsymbol{R} = \boldsymbol{R}_A + \boldsymbol{r} \tag{1b}$$

Taking the substantial derivative of Eqs. (1) we obtain the velocity of any fluid particle with respect to the G-F frame; that is,

$$\boldsymbol{V} = \boldsymbol{V}_A + \boldsymbol{\Omega}\times\boldsymbol{r} + \boldsymbol{v} \tag{2}$$

where $\boldsymbol{V}_A$ is the velocity of the origin A, $\boldsymbol{\Omega}$ is the angular velocity of the B-F frame, and $\boldsymbol{v}$ is the velocity of the fluid particle relative to the B-F frame. The components of the angular velocity in the B-F frame can be expressed in terms of the derivatives of the Euler angles.

Later we will need to transform partial derivatives from one coordinate system to the other. The needed relationships are developed next. We denote with $\Phi(\boldsymbol{R},t)$ the potential function that is expressed in terms of the absolute position vector $\boldsymbol{R}$

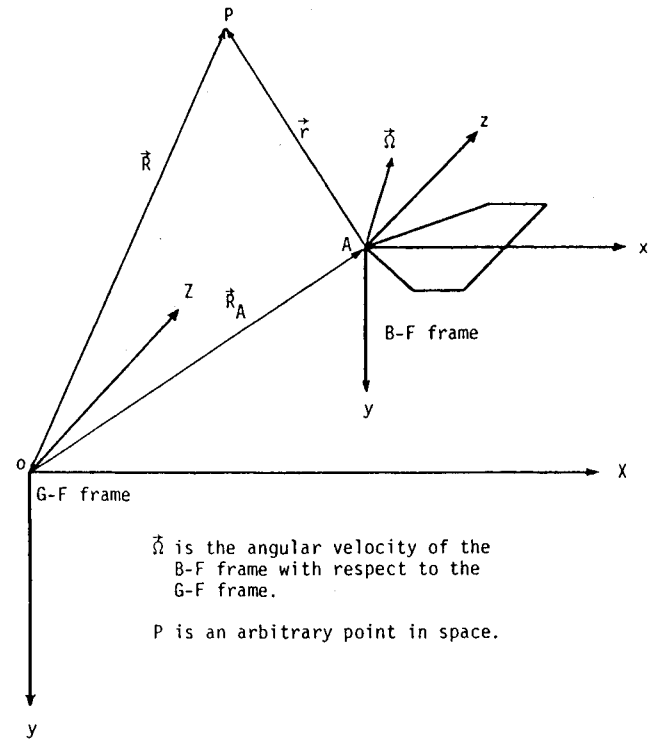

Fig. 1 Two coordinate systems.

and time t and with $\phi(r,t)$, the potential function that is expressed in terms of the relative position vector $\boldsymbol{B}$ and time t.

It can be shown that[8]

$$\nabla_R \Phi = \nabla_r \phi \tag{3}$$

Taking the partial derivatives with respect to time, we may want to hold either $\boldsymbol{R}$ or r constant. The relationship between the two time derivatives is given by

$$\frac{\partial \Phi}{\partial t}\Big|_R = \frac{\partial \phi}{\partial t}\Big|_r - \nabla_r \phi \cdot (V_A + \Omega \times r) \tag{4}$$

B. The Mathematical Problem

We are modeling the flow around a thin finite wing of arbitrary planform, moving through an inviscid incompressible fluid. As the wing moves, it sets the fluid in motion; as a result, vorticity is created in the boundary layers of the upper and the lower surfaces and vortices are formed along the sharp edges. The latter are shed and convected away from the wing and form the wake. In the model we restrict all the vorticity in the flow to a thin region around the lifting surface and its wake and consider the flow outside this region to be irrotational.

We consider the wing and the wake to be a sheet of vorticity that consists of two parts: the bound-vortex sheet that represents the wing and the free-vortex sheet that represents the wake. The position of the first is specified; as a result a finite pressure jump exists across it in general. The position of the second is not specified a priori; it is allowed to deform freely during the solution until it assumes a force-free position. As a result, there is no pressure jump across it. The two parts of the vortex sheet are joined along the sharp edges where separation occurs, the same edges where the Kutta condition is imposed in a steady flow. In the mathematical model we represent the vortex sheet by a lattice of discrete vortex lines.

The total velocity field generated by the vorticity must satisfy the continuity equation, which for an incompressible fluid is

$$\nabla \cdot V = 0 \tag{5}$$

The velocity is computed according to the Biot-Savart law; thus, condition (5) is satisfied identically. In addition to Eq. (5) the flow must satisfy the following:

1) Condition at infinity:

$$|V| \to 0 \text{ away from } S_{LS} \text{ and } S_W \tag{6}$$

where S_{LS} denotes the lifting surface and S_W the wake surface. The condition at infinity is satisfied identically because the velocity generated by the disturbance is computed according to the Biot-Savart law.

2) No-penetration condition:

$$(V - V_{LS}) \cdot n = 0 \text{ on } S_{LS} \tag{7}$$

where V is the absolute velocity of the fluid particle, V_{LS} is the velocity of the lifting surface, and n is the unit normal vector. In general, V_{LS} varies in space and time.

3) Continuous pressure in the wake: for an inviscid fluid, the Kelvin-Helmholtz theorem requires that all vorticity be transported with the fluid particles when the pressure is continuous. Hence,

$$\frac{D\Gamma}{Dt} = 0 \text{ on } S_W \tag{8}$$

where Γ is the circulation around any arbitrary closed loop and D/Dt is the substantial derivative. This condition is used to obtain the position of the force-free wake.

4) Spatial conservation of circulation.

5) Unsteady Kutta condition: all the vorticity generated along the sharp edges where the steady-state Kutta condition is enforced is shed.

In the unsteady vortex-lattice method, we replace the vortex sheet, bound and free parts, by a lattice of short, straight vortex segments which divide the lifting surface into a number of elements of area. This is shown in Fig. 2. Experience with the vortex-lattice method suggests that the geometric shape of the elements in the lattice affects the accuracy slightly and the rate of convergence (for steady flows) considerably. In an earlier paper, Mook and Maddox[9] extended a code developed by Giesing et al.,[10] which used tapered panels to include a leading-edge vortex system. Subsequently, Kandil et al.,[11] developed a code based on rectangular elements, and Kelly[12] systematically experimented with various user-chosen parameters (such as the arrangement of the lattice). As a result of these efforts, we conclude that rectangular elements work better (slightly better in some cases) than other shapes. Consequently, we use rectangular elements everywhere except along the leading edges of delta wings where we are forced to use triangular elements. In order to guarantee the spatial conservation of circulation, we take the circulation to be the same for all the discrete vortex segments of the same loop. These circulations are denoted by G_i. We note that each of the straight segments (except in the leading row) is formed from parts of two loops. For example, the circulation around the segment AB in Fig. 2c is given by G_1-G_7.

Experience has shown that best results are obtained when the extensions along the leading edge are in the plane of the wing and perpendicular to the leading edge (this also seems to be shown by the experimental data of Hummel[13]) and have a length equal to the span of an area element. This placement of the extensions may be regarded as part of the Kutta condition.

Because we approximated the vortex sheet with a lattice, we can satisfy the no-penetration condition of Eq. (7) at only a finite number of points, the control points of the bound lattice. In Fig. 2, the control point is the centroid of the corner points for a rectangular element and the midpoint between the nodes along the leading edge. The unit normal vector of each element is obtained from the cross product of the two diagonals. The problem is to find the circulations (around the loops of discrete vorticity that generate the flow) satisfying conditions (2) at the control points (3) and (5).

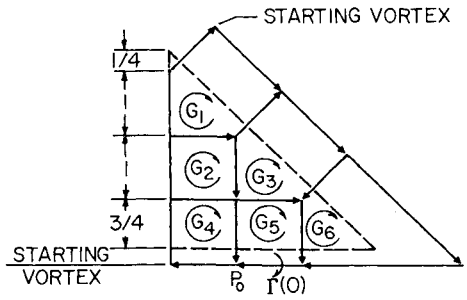

a) Just after the start of the motion.

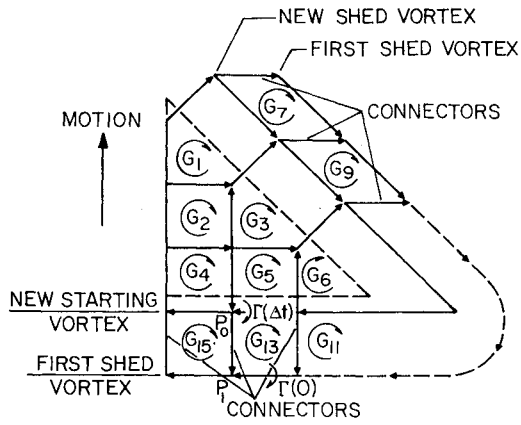

b) After one time step.

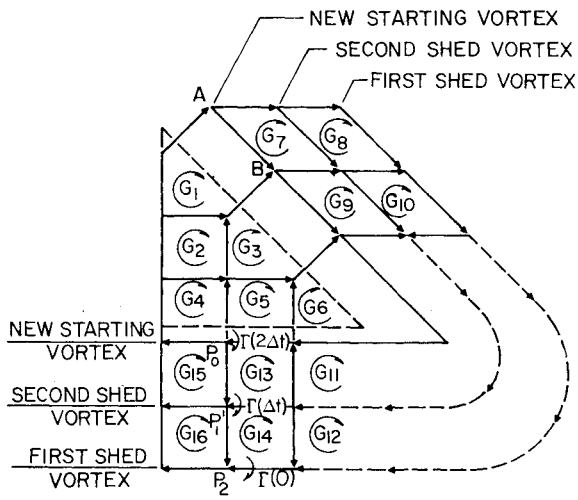

c) After two time steps.

Fig. 2 Schematic of the vortex lattice for an impulsively started delta wing.

C. Example of an Impulsive Start

The computational procedure is best explained by means of an example. To this end we consider a flat delta wing that impulsively starts to move through a fluid at rest. The velocity is parallel to the ground, in the X direction, and constant. A lattice of 3×6 elements simulates the wing; Fig. 2 shows half of the lattice. Before the motion begins, we set all the circulations equal to zero. At $t=0$ the instant motion begins and the circulations in the bound portion of the vortex lattice change instantaneously. A discrete vortex line is formed along the sharp edges, as Fig. 2a shows; it represents the starting vortex described by Prandtl.[15] The existence of the starting vortex is dictated by the requirement of spatial conservation of circulation.

Vorticity is convected into the wake from the sharp edges of the wing at the particle velocity ($D\Gamma/Dt=0$). At the instant motion begins, no vorticity has been convected; thus, there is no wake.

In order to find the circulations, we construct a matrix of influence coefficients A_{ij} for $i, j=1, 2, \ldots, N$ where N is the number of elements in the bound lattice. The coefficient A_{ij} represents the normal component of the velocity at the control point of the ith element induced by the closed loop of vorticity around the jth element having unit circulation. Multiplying A_{ij} by the actual circulation for the jth element, G_j, and then summing for all j, we obtain the normal component of the velocity at the control point of the ith element induced by all the bound vortices. Therefore,

$$\sum_{j=1}^{N} A_{ij}G_j(0) = [V_{LS}(0)\cdot n]_i \qquad \text{for } i=1, 2, \ldots, N \tag{9}$$

where n_i is the normal vector at the control point of the ith element. The velocities and the circulations are functions of time. In this example, the wing is not deforming; hence, the nodes in the bound lattice are fixed. Control points, relative positions, normal vectors, and the influence coefficients remain constant. In general, however, the wing does deform and the A_{ij} must be computed at each time step.

The system of Eq. (9) is solved for the unknown circulations by an interative procedure. For subsequent time steps, the values of G_j from the previous time step are used as the initial guess. These are generally quite close to the correct values, and convergence is therefore achieved rapidly.

At the next time step, $t=\Delta t$, we convect the entire starting vortex at the local particle velocity. The local velocity relative to the moving frame is computed at each node of the discrete vortex line along the leading and trailing edges from

$$v = V - V_A - \Omega\times r \tag{10}$$

where V is the absolute velocity calculated from the Biot-Savart law and v is the relative velocity. Because all these quantities are functions of time, the question of which instantaneous quantities to use is raised. There are several options: for example, we can use the quantities that were calculated at the previous time step ($t=0$), the quantities at the present time step ($t=\Delta t$), or their averaged values for the two time steps. In all cases except the first, iteration is needed, which increases the computation time. In all cases considered, we found the first option to be stable, but we do not know of any analysis that shows it to be stable in every case. In several comparisons, we found very little difference in the computed results for the various options; therefore, the first option was used to compute all the results in this paper.

In Fig. 3a, we see the side view of the wing shown in Fig. 2a. The starting vortex at the trailing edge is represented by a dot at P_0, with a circulation $\Gamma(0)$. At the next time step, Figs. 2b and 3b, the starting vortex is convected to the new position denoted by P_1 in Fig. 3b. The circulation is still $\Gamma(0)$ in order to satisfy temporal conservation of circulation. Simultaneously, a new starting vortex is formed at P_0 in Fig. 3b, with a circulation $\Gamma(\Delta t)$. In order to satisfy spatial conservation of circulation, we must join the two starting vortices at the nodal points with the connectors shown in Figs. 2b and 3b. The connectors are discussed below. The length and direction of the connectors are computed from Eq. (10):

$$(P_0P_1) = v_0(0)\Delta t \tag{11}$$

Now we calculate the bound circulations for the time $t=\Delta t$. Equations (9) are no longer valid because they do not take the existence of the wake into account. Hence, condition (7) must be expressed as follows:

$$\sum_{j=1}^{N} A_{ij}G_j(\Delta t) = [V_{LS}(\Delta t) - V_W(\Delta t)]\cdot n_i \text{ for } 1,2,\ldots, N \tag{12}$$

where V_W is the velocity induced by the wake, whose position and circulation distribution are known. After we calculate

$G_j(\Delta t)$ from Eqs. (12), we proceed to the next time step, $t=2\Delta t$.

Figure 2c and 3c show the wake after two time steps—the new positions of the two previously shed vortices and the newly formed starting vortex. There is no vorticity along the lines from P_0 to P_1 and from P_1 to P_2. During the second time step, all the vorticity that lay along the line from P_0 to P_1 was convected by the motion and now lies along the line from P_1' to P_2. The broken lines with arrows represent this migration.

In the present model, all the starting vorticity generated at each time step is shed and convected. Referring to Figs. 2 again, we see that this is accomplished by simply convecting the entire closed loop of vorticity from the elements along the sharp edges of the bound lattice into the wake. Thus, the value of G_{15} in Fig. 2b, which represents the situation after one time step, is the same as the value of G_4 in Fig. 2a, which represents the situation at the onset of the motion. And the value of G_{16} in Fig. 2c, which represents the situation after two time steps, is the same as the value of G_{15} in Fig. 2b. The value of G_{15} in Fig. 2c is the same as the value of G_4 in Fig. 2b.

Because the vorticity varies along the edges (e.g., $G_5 \neq G_4$, and hence $G_{15} \neq G_{13}$ and $G_{16} \neq G_{14}$), the vorticity along the connectors is not zero. For example, in Fig. 2c, the circulation around the line from P_0 to P_1' is $G_{15}-G_{13}$, while the circulation around the line from P_1' to P_2 is $G_{16}-G_{14}$.

The procedure described above can be continued for any desired number of steps. At each new time step, a new starting vortex is formed, shed, and convected away from the edge. When these vortices are so far away that they do not have any appreciable influence on the flow around the lifting surface, they are neglected.

It is desirable to have uniform elements in the lattice. In the present scheme, we choose the characteristic length L to be the chord of the rectangular elements in the bound lattice and the time step to be $\Delta t = L/U$, where U is a speed characterizing the forward motion of the lifting surface. As a result, the streamwise lengths of the elements in the wake are approximately the same as the chordwise length in the bound lattice. Moreover, changes in the number of elements of the bound lattice are automatically accompanied by corresponding changes in the time step.

In Fig. 4 we present an actual solution showing how the wake develops for delta wings after an impulsive start. The solutions are after one, three, and five time steps, and the steady-state solution ($t=\infty$) is also given. The first segment of each vortex line in the wake emanating from the leading edge lies in the plane of the wing and is perpendicular to the leading edge. All the other segments in each line have their positions determined as part of the solution. What appear to be triangles along the leading edges in the planviews of Fig. 4 are actually formed by the leading edge (which is not a vortex line), the first segment of the vortex line (which lies in the plane of the wing), and the projections of the next one or two segments, which are rising above the plane of the wing (as the elevations in Fig. 4 indicate) and which are nearly parallel to the midspan chord.

The flow in Fig. 4 is symmetric, but symmetry is not a requirement. Figure 5 shows the steady state for the same wing at an angle of yaw. In the steady state, the streamwise vortex lines in the wake coincide with streamlines, and the circulation around the cross-flow lines in zero. These conditions emerge naturally from the general unsteady process when the motion of the lifting surface is uniform.

This example considered an impulsively started wing, but the method can accommodate any complete description (circulations and positions) of the wake as an initial condition.

D. Computation of the Aerodynamic Loads

The force on each area element of the bound lattice is calculated by determining the pressure jump across the lifting surface at the control point and then multiplying it by the area of the element. The total force and moments are then calculated. The pressure is calculated from Bernoulli's equation for unsteady flows.

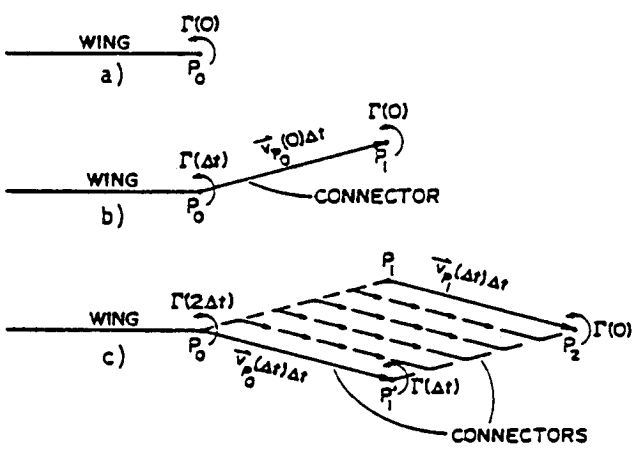

Fig. 3 Convection of shed vortices a) just after the start of the motion, b) after one time step, c) after two time steps.

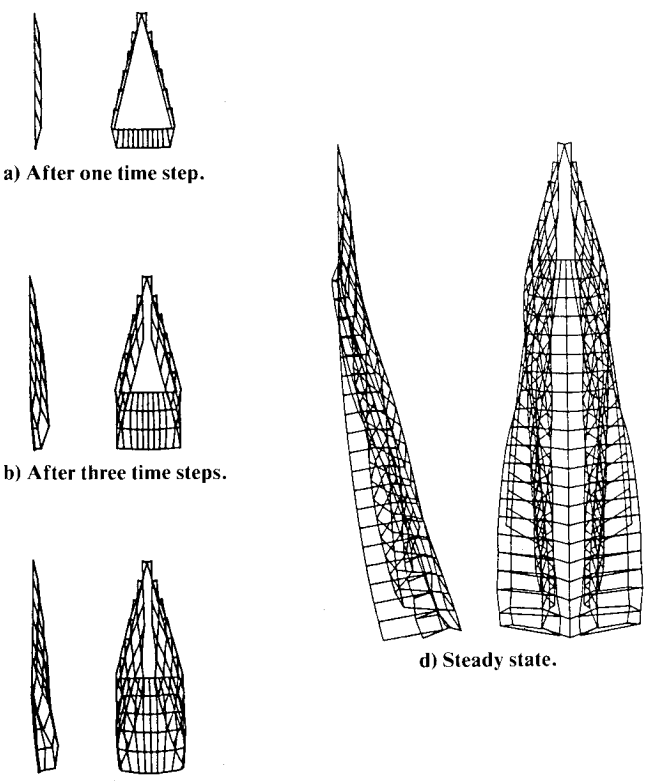

Fig. 4 Representation of the actual vortex-lattice for an impulsively started delta wing.

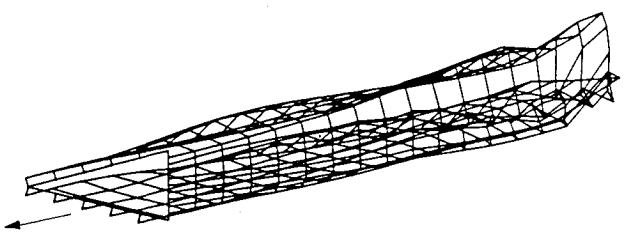

Fig. 5 Steady-state solution for flow over a delta wing of unit aspect ratio at 15 deg angle of attack and 15 deg angle of yaw.

For element i, the difference between the pressure coefficients on the upper and lower surfaces at the control point is given by

$$\Delta Cp_i = -2\frac{\partial G_i}{\partial t} - 2[\Delta V \cdot (V_m - V_A - \Omega \times r)]_i \qquad (13)$$

where G_i is the loop circulation discussed above, V_m the velocity generated by all the vortex elements (the mean velocity), and ΔV the discontinuity in the tangential component caused by the local vorticity. The local vorticity is discussed next.

The average circulation around the discrete vortex segments on parallel edges of an element is considered to be the circulation around a sheet of vorticity parallel to and between the same edges. (The vorticity is concentrated into cores to facilitate computation of the velocity field). Thus, this average circulation is related to the jump in the tangential component of velocity perpendicular to these edges, across the thickness of the lifting surface. More details can be found in Refs. 2 and 14.

III. Applications

In this section we apply the method to several examples, which include both steady and unsteady flows. These examples partially illustrate the range of planforms, angles of attack, and maneuvers that can be treated. All the steady flows were calculated by giving the wing an impulsive start and then having it move at constant velocity until a steady state developed.

For steady flows, the normal-force and pitching-moment coefficients predicted by the present method are in excellent agreement with those predicted by the steady flow code (see Kandil et al.[11]), with the experimental data of Peckham[16] for delta wings, and Belotserkovskii[17] for rectangular wings.

Because the present method is capable of predicting the roll moment C_l due to yaw β, it can be used to calculate the stability derivative $dC_l/d\beta$. In Table 1, the values of C_l are given as functions of angle of attack for three yaw angles. Finite-difference formulas were used to compute the stability derivative $dC_l/d\beta$ as a function of angle of attack. The experimental results of Peckham[16] are also given. There is excellent agreement.

In Fig. 6, we show the steady-state positions of the vortex lines for symmetric flow over a cropped delta wing. In Fig. 7, the lift, drag, and pitching moment for the cropped delta wing are compared with the theoretical predictions and the experimental observations of Lamar.[18] Lamar's predictions were obtained by a procedure based on the leading-edge suction analogy. The angle of sweep of the leading edge is 63 deg; the taper ratio is 0.4.

In Fig. 8, we show the delta wing of Fig. 4 executing a roll. The wing is rolling about the midspan axis and the angle of attack is zero. One side of the wake is always above the wing and the other is always below; the plan is always symmetrical. The wing was started impulsively and made to roll at a constant rate until a steady state developed. In Fig. 9, the roll-moment coefficients are shown as functions of time for

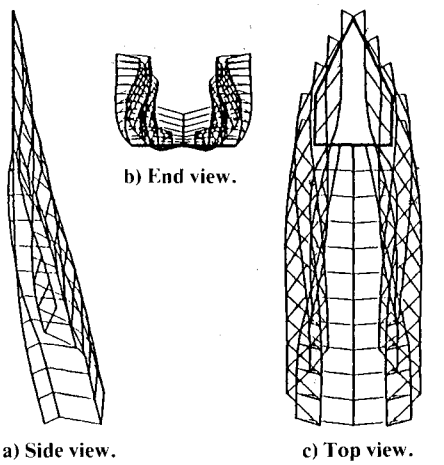

Fig. 6 Steady-state solution for flow over a cropped delta wing at 15 deg angle of attack.

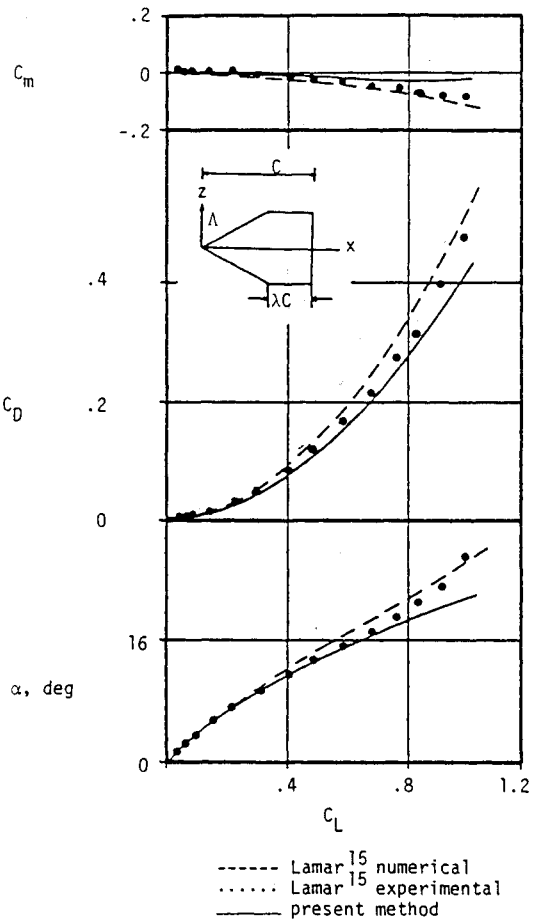

Fig. 7 The lift, drag, and pitching moment coefficients for a cropped delta wing with an angle of sweep Λ = 63 deg , taper ratio λ = 0.4.

Table 1 Stability derivative for various angles of attack for a delta wing of aspect ratio one

α, deg	C_l $\beta=0$	C_l $\beta=\pm2$ deg	C_l $\beta=\pm4$ deg	$\left.\frac{dC_l}{d\beta}\right\|_{\beta=0}$	$\left.\frac{dC_l}{d\beta}\right\|_{\beta=0}$ [a]
0.00	0	0.00000	0.00000	0.000	0.009
6.11	0	0.00396	0.00702	0.107	0.096
12.26	0	0.00756	0.01332	0.204	0.200
18.44	0	0.00916	0.01976	0.273	0.277

[a] Peckham's experimental results.

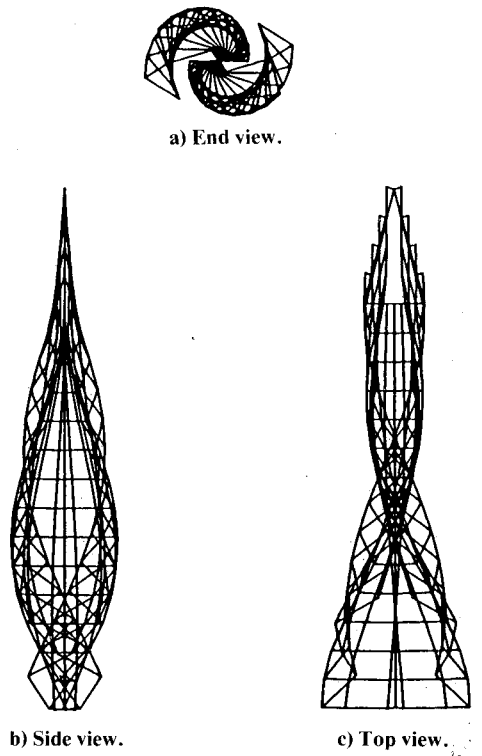

Fig. 8 Steady-state solution for flow over a delta wing of unit aspect ratio at 0 deg angle of attack executing a fast roll about its midspan axis.

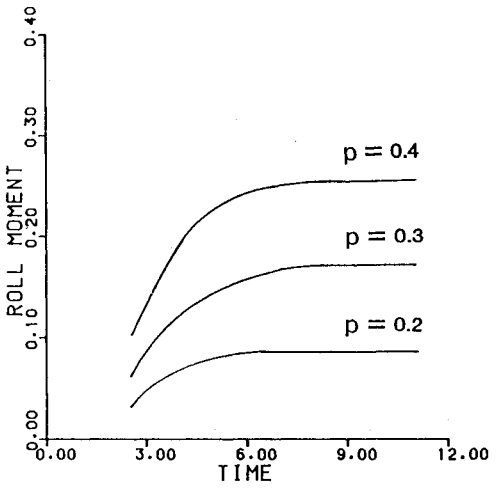

Fig. 9 Roll-moment coefficient C_l as a function of time t for different roll rates p.

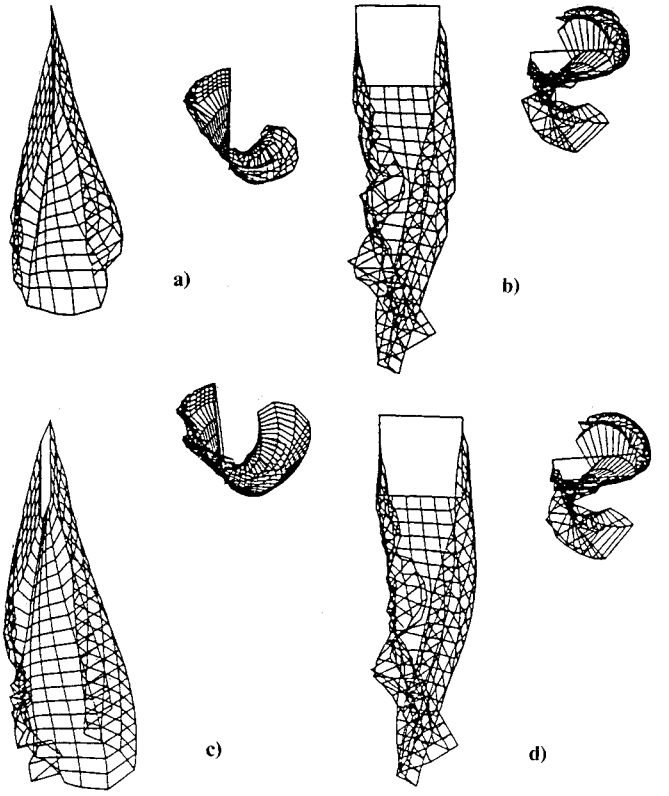

Fig. 10 The unsteady solution for flow over a rectangular wing at 15 deg angle of attack, executing a roll about its midspan axis.

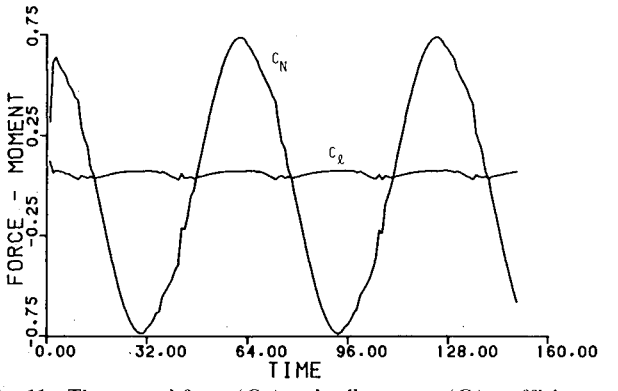

Fig. 11 The normal-force (C_N) and roll-moment (C_l) coefficients as functions of time for a rectangular wing at 15 deg angle of attack, executing a roll about its midspan axis. The roll angle is $\phi = (0.1)t$.

several roll rates. The steady state develops more rapidly at the lower roll rates.

In Fig. 10, the vortex lines in the wake of the rectangular wing are shown in another roll maneuver. Here the roll axis is the midspan chord as before, but here this axis is at 15 deg angle of attack. The two views are from straight above and straight ahead. As the wing rotates, the wing tip vortex periodically collapses and partially changes sides. In Fig. 11, the roll-moment and normal-force coefficients are shown as functions of time for these revolutions. The slight aberrations in the loads are numerically generated by the collapsing, partial changing of sides, and reestablishing of the wing-tip vortex systems during complete revolutions. From these histories of position, force, and moment, it is possible to determine the phase differences.

Finally, we consider the loads on a rectangular wing with large flaps when the flaps oscillate periodically in unison. In Fig. 12, the steady-state solution is depicted. In Fig. 13, the flap angle, normal-force coefficient, and pitching-moment coefficient are plotted as functions of time. The angle of attack of the wing remains constant at 15 deg. The irregularities in the loads (slight in the plot of C_N and pronounced in the plot of C_{M_p}) correspond to just after the upward passage of the flap through the plane of the lifting surface and are probably caused by the strong interaction of the flaps with the wing-tip and trailing-edge wakes. The present program yields some aberration, but it is unlikely that these are accurate simulations of the actual flow. The loads are periodic, but they do not appear to be simple harmonic as the motion of the flap is. Moreover, the loads are not in phase with each other, nor is either load in phase with the flap. As the flaps moved downward, the effective camber is changing

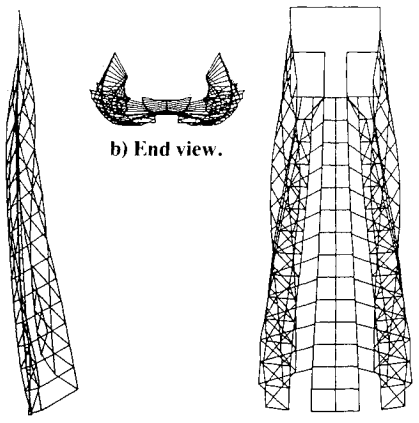

Fig. 12 Steady-state solution for flow over a rectangular wing with flaps at 15 deg angle of attack and 10 deg flap deflection.

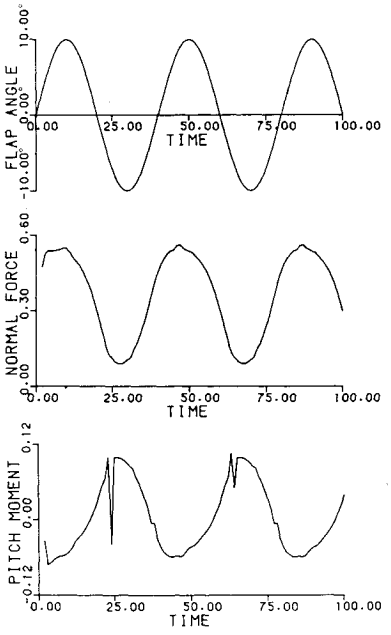

Fig. 13 Variation of flap-deflection angle β, normal-force and pitching-moment coefficients with time.

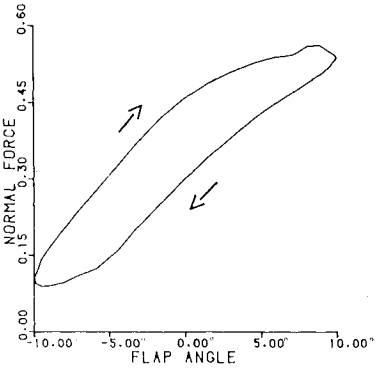

Fig. 14 Demonstration of the hysteretic behavior of the normal-force coefficient.

while the apparent downwash is increasing (the latter due to two effects—increases in the angle of attack and the motion of the wing). The maximum load occurs before the flaps are fully deflected downward, and the minimum load occurs before the flaps are fully deflected upward. In Fig. 14, the normal-force coefficient is shown as a function of flap angle. The arrows indicate the passage of the point representing the solution with time. The well-known hysteretic behavior is clearly predicted.

IV. Conclusions

In the present paper, we described an extension of the familiar vortex-lattice method that can treat general, unsteady lifting flows. The general procedure treats steady flows more efficiently than our specialized steady flow, vortex-lattice procedure.

In all cases where comparisons with experimental and other numerical results are possible, the present procedure predicts the loads very accurately. The numerical examples partially illustrate the range of application.

Acknowledgment

This research was supported by the Office of Naval Research under Contract N00014-79-C-0103 and NASA under Grant NSG-1262.

References

[1] Thrasher, D. F., Mook, D. T., Nayfeh, A. H., and Kandil, O. A., "Application of the Vortex-Lattice Concept to General, Unsteady Lifting-Surface Problems," AIAA Paper 77-1157, 1977.

[2] Konstadinopoulos, P., Mook, D. T., and Nayfeh, A. H., "A Numerical Method for General Unsteady Aerodynamics," AIAA Paper 81-1877, 1981.

[3] Ashley, H. and Rodden, W. P., "Wing-Body Aerodynamic Interaction," *Annual Review of Fluid Mechanics,* Vol. 4, 1972, pp. 431-472.

[4] Belotserkovskii, S. M., "Study of the Unsteady Aerodynamics of Lifting Surfaces Using the Computer," *Annual Review of Fluid Mechanics,* Vol. 9, 1977, pp. 469-494.

[5] Ueda, T. and Dowell, E. H., "A New Solution Method for Lifting Surfaces in Subsonic Flow," *AIAA Journal,* Vol. 30, March 1982, pp. 348-355.

[6] Levin, D. and Katz, J., "Vortex-Lattice Method for the Calculation of the Nonsteady Separated Flow over Delta Wings," *Journal of Aircraft,* Vol. 18, Dec. 1981, pp. 1032-1037.

[7] Kandil, O. A., "State of the Art of Nonlinear Discrete-Vortex Methods for Steady and Unsteady High Angles of Attack Aerodynamics," AGARD CP-247, Jan. 1979.

[8] Karamcheti, K., *Principles of Ideal-Fluid Aerodynamics,* John Wiley and Sons, Inc., New York, 1966.

[9] Mook, D. T. and Maddox, S. A., "Extension of a Vortex-Lattice Method to Include the Effects of Leading-Edge Separation," *Journal of Aircraft,* Vol. 11, Feb. 1974, pp. 127-128.

[10] Giesing, J. P., Kalman, T. P., and Rodden, W. P., "Subsonic Unsteady Aerodynamics for General Configurations," AF Tech. Report AFFDL-TR-71-5, Pt. 1, Vol. 2, Air Force Flight Dynamics Lab., Wright-Patterson AFB, Ohio, Nov. 1971.

[11] Kandil, O. A., Mook, D. T., and Nayfeh, A. H., "Nonlinear Prediction of the Aerodynamic Loads on Lifting Surfaces," *Journal of Aircraft,* Vol. 13, Jan. 1976, pp. 22-28.

[12] Kelly, S. G., "A Systematic Investigation of the Parameters Affecting the Accuracy of the Vortex-Lattice Method," M. S. Thesis, Dept. of Engineering Mechanics, Virginia Polytechnic Institute and State University, Blacksburg, Va., May 1977.

[13] Hummel, D., "On Vortex Formation Over a Slender Wing at Large Angles of Incidence," AGARD CP-247, Jan. 1979.

[14] Konstadinopoulos, P., "A Vortex-Lattice Method for General, Unsteady, Subsonic Aerodynamics," M. S. Thesis, Dept. of Engineering Mechanics, Virginia Polytechnic Institute and State University, Blacksburg, Va., July 1981.

[15] Prandtl, L. and Tietjens, O. G., *Applied Hydro- and Aeromechanics,* Dover Press, 1957.

[16] Peckham, D. H., "Low-Speed Wind-Tunnel Tests on a Series of Uncambered Slender Pointed Wings with Sharp Edges," *Reports and Memoranda,* No. 3186, Dec. 1958.

[17] Belotserkovskii, S. M., "Calculation of the Flow Around Wings of Arbitrary Planform in a Wide Range of Angles of Attack," NASA TT F-12, 291, 1969.

[18] Lamar, J. E., "Extension of Leading-Edge Suction Analogy to Wings with Separated Flow Around the Side Edges At Subsonic Speeds," NASA-TR-R-428, Oct. 1974.